Forces in Mechanics 21 (2025) 100337

Contents lists available at ScienceDirect

Forces in Mechanics

journal homepage: www.sciencedirect.com/journal/forces-in-mechanics

# Elastic-damage characterization of fibre-bundle lamina of CFRP composite through 3D digital image correlation and finite element method

S. S. R. Koloor [a,b,*], A. Farokhi Nejad [c], N. Yidris [b,*], S.M. Sapuan [d], M.R. Abdullah [c], M.N. Tamin [c]

[a] Faculty of Mechanical Engineering, Universität der Bundeswehr München, Werner-Heisenberg-Weg 39, Neubiberg, Munich 85579, Germany
[b] Department of Aerospace Engineering, Universiti Putra Malaysia, UPM Serdang, Selangor Darul Ehsan 43400, Malaysia
[c] Faculty of Mechanical Engineering, Universiti Teknologi Malaysia, Johor Bahru 81310, Malaysia
[d] Department of Mechanical Engineering, Universiti Putra Malaysia, UPM Serdang, Selangor Darul Ehsan 43400, Malaysia

ARTICLE INFO

*Keywords:*
CFRP composite laminate
Carbon fiber damage evolution
Continuum damage mechanics
Finite element simulation
3D digital image correlation

ABSTRACT

Carbon fibers' exceptional mechanical properties make them the major load-bearing component of CFRP composites, which are rapidly being used in modern aerospace applications. Design of multi-directionally (MD) laminated composite structures for specific operational load requires the exact determination and force analysis of 0°-laminas and their arrangement in the lamina assembly process. The significant property variation between carbon fibers and matrix components indicates that the mechanical behavior of the 0°-laminas is attributed largely to the fiber-bundle at the mesoscale. The elastic properties of fiber have been obtained through standard tests, however, many challenges are encountered in the characterization of fiber damage and fracture processes. In this research, a new experiment is introduced where tensile tests are performed on single edge-notch 0°-CFRP composite monitored by 3D digital image correlation (DIC), to demonstrate the mechanism of deformation and failure and determine the exact elastic-damage properties. A hybrid experimental-computational approach is developed where finite element models representing the experiment, are used to obtain and validate the damage evolution characteristics of fibers in CFRP lamina. In addition, test and simulation results are utilized to describe the mechanism and mechanics of deformation and damage of the composite structure.

## 1. Introduction

The excellent mechanical features of carbon fiber-reinforced polymer (CFRP) composites have made this material an excellent choice for the design of aerospace structures. Fibers are the load-bearing constituent of composite materials, which are subjected to various damages, including cracking, shearing, or buckling phenomena [1,2]. Therefore, mechanical characterization of the unidirectional (UD) lamina in the fiber direction (0°-lamina) is an important matter to predict the yielding and strength limit of the composite for design issues of composite structures. In continuum damage mechanics [3,4], the required properties to address UD lamina behavior in the 0-direction include elastic modulus, strength, fracture energy, and failure strain variables. In practice, the elastic properties of 0°-lamina have been extracted using standard test methods by simple tensile tests [5,6], however, many challenges are encountered in obtaining the fracture behavior of UD composite, including the illustration of the mechanism of damage process, determination of fracture energy, and also failure strain limit. In this regard, the standard test method to obtain the translaminar fracture toughness of laminated composites indicates the validity of the test only for laminates that produce a small damage zone [7], while fiber fracture events normally occur on a large scale and at a glance. Many of the previous investigations indicated that the translaminar fracture testing to obtain 0°-lamina fracture energy is not yet mature, and the experimental scenarios are challenging to conduct [8,9]. The use of cross-ply specimens is also practiced for testing, which reduces the accuracy of the results by including the effect of angle laminas in the measured data [10]. When a more detailed examination of a single carbon fiber is conducted, it becomes quite intriguing to note that its critical strain energy release rate can be exceptionally low, estimated at a mere 7.4 $J/m^2$ [11]. However, within a composite material, this condition undergoes tremendous modification. A significant part of the strain energy is dissipated during composite failure [12]. This energy release is strongly related to processes such as fiber-matrix debonding and the

* Corresponding authors.
*E-mail addresses:* seyed.rahimian@unibw.de (S.S. R. Koloor), nyidris@upm.edu.my (N. Yidris).

https://doi.org/10.1016/j.finmec.2025.100337
Received 24 June 2024; Received in revised form 28 September 2025; Accepted 19 October 2025
Available online 21 October 2025

subsequent pull-out of individual fibers, which is revealed on the fracture surface [13,14]. Collectively, these factors contribute to ply-level fracture toughness that is more than three times greater than that of a single fiber. When a compressive loading is applied in the fiber direction, the possible failure will be in two ways: shear-driven fiber failure or fiber kinking. The precise form of failure seen is determined by elements such as the existence of shear loads, which might occur as a result of localized fiber misalignment. Shear failure causes bending ahead of the fracture point, which eventually results in fiber kinking failure [15,16].

An intralaminar crack occurs entirely within a single ply, usually parallel to the fibers. It can be caused by a variety of factors, including fiber breakage, matrix cracking, and fiber-matrix debonding. Interlaminar cracks, as opposed to those that occur within a single ply, occur between the plies. They are essentially layer separations that are frequently caused by shear stresses, impact damage, and defects in production. Translaminar cracks, on the other hand, penetrate the whole thickness of the laminate, potentially initiating an intralaminar or interlaminar crack and propagating through several plies. The fracture surface produced by intralaminar matrix cracking that grows longitudinally emphasizes that the estimated toughness of such failure modes is close to that of their interlaminar counterparts [17,18]. The critical strain energy release rates correlated to such failures are inherent material features that necessitate extensive characterization to fully comprehend the damage tolerance of the material system under investigation. The primary focus in the characterization of translaminar fracture is on toughness measurement of multidirectional laminates made from UD or 2D woven composite material structures [19,20]. In such conditions, the determined toughness is influenced by the lay-up configuration and results from a large number of constituent plies failing in combinations of the aforementioned failure causes. Only those tests associated with compact tension, three/four-point bending experiment, and extended compact tension tests show stable crack propagation in the samples among the numerous specimen configurations used in the literature [21–23]. Crack growth stability is crucial for generating resistance curves (R-curves), which track variations in the critical strain energy release rate as damage evolves. Compact Tension (CT) is extensively used for assessing translaminar fracture toughness in composite materials. This configuration has been widely employed for characterizing laminates comprising a diverse range of materials, including carbon/epoxy, carbon/carbon, carbon/PEEK, and boron/aluminum. A common approach for data analysis involves calculating the critical stress intensity factor, $K_{Ic}$, following the ASTM E399 guidelines for metallic materials [24]. Nevertheless, it's important to note that these attributes, which are dependent on the lay-up, have limited practical utility since they don't capture intrinsic material qualities. Several studies introduced the concept of an intrinsic material property known as $K_{Ic0}$, which represents the fracture toughness of the 0°-lamina within a composite laminate, irrespective of the lay-up configuration [25,26]. This concept draws from classical lamination theory, where the stress endured by the 0°-lamina in a laminated composite ($\sigma_{0c}$) is related to the applied stress on the laminate ($\sigma_c$) through the layer elastic property. Notably, this same parameter connects $K_{Ic}$ and $K_{Ic0}$, underscoring that $K_{Ic0}$ is indeed an intrinsic material attribute. In order to determine the fracture toughness related to translaminar tensile and compressive failure modes, researchers have employed diverse methods and specimen configurations. These studies have yielded invaluable insights into the behavior of composites subjected to various loading conditions [27].

The 3D Digital Image Correlation (DIC) method is included as one of the new advancements to the known 2D DIC, highlighted with additional features such as the ability to characterize composites using full-field measurement of deformation and strain with precision at the micro-level [27]. This is due to the difficulties in manufacturing of FRP composite structure through prepreg layup, Towpreg fibre winding, or even automated fibre placement by robots, etc., which creates the composite surface very rough with meso-scale 3D bumps, resulting in imprecision when 2D DIC is used to measure deformation and strain at a specified surface. On the other hand, 3D DIC uses two cameras [28] with specially adjusted parameters to capture and resolve the error of surface roughness, and provide accurate measurement of the strain field on the composite surface [29].

Literature study highlights the lack of research and technical difficulties in the determination of fracture properties of 0° CFRP lamina, in which the limitation of the standard method for full characterization of UD lamina properties is discussed. Considering the gap of study in the proper determination of fiber-bundle properties in the form of the 0°-FRP lamina in elastic to damage states, this study aimed at using 3D DIC system capability to capture the true strain field at the surface and around the notch tip of specially prepared CFRP laminate specimen, to record/measure the mechanism of deformation to fracture of the CFRP composite. The DIC result, along with the experimental data of the CFRP composite structure subjected to tensile load, are used to explain the complex behavior of the structure and illustrate the mechanism of composite deformation before the fracture state, which is later used for the measurement of fracture energy and failure parameters of 0° CFRP lamina. Using the proposed experimental-numerical approach, validated FE models of the experimental cases are employed to examine the accuracy of the mechanical properties, including the fracture energy parameter, which led to full characterization of the 0°-FRP lamina. In addition, this innovative approach and results provided an insight into the mechanics of deformation and the mechanism of damage of 0°-CFRP composite. It is concluded that the method can be applicable to characterize other fibrous composites where the mechanical behavior of the structure is dependent on reinforcement constituents and their arrangement in the composite system.

## 2. Continuum damage mechanics of 0°-lamina failure

The 0°-lamina is treated as an equivalent orthotropic ply with greater mechanical properties in the fiber direction. The constitutive model response of the composite material at the local point is represented by a bilinear softening law for fiber fracture damage mode, as depicted in Fig. 1. In this model, the elastic properties and strength could be obtained using a standard test [28], while the fiber fracture energy ($G_{CF}$), deformation and fracture, and the damage softening form could potentially be determined using the DIC method.

Considering lamina behavior on fiber direction, the stress-strain behavior within the elastic regime could be determined using orthotropic Hooke's law [29], while damage initiation is predicted using a quadratic relation [14]:

$$\left(\frac{\widehat{\sigma_{11}}}{X^T}\right)^2 + \left(\frac{\widehat{\tau_{12}}}{S^L}\right)^2 = {d_f^t}^2 \tag{1}$$

where $\widehat{\sigma_{11}}$ and $\widehat{\tau_{12}}$ are the effective normal and shear stresses within the elastic regime, generated in the lamina under tension, and $X^T$ & $S^L$ are the constant values corresponding normal and shear strength of the lamina, while the parameter $d_f^t$ Indicate the fiber damage initiation in the lamina in tensile conditions. The displacement at fracture of the lamina in the fiber direction is computed using [13]:

$$\delta_{eq}^f = \frac{2\sqrt{{\varepsilon_{11}^o}^2 + {\varepsilon_{12}^o}^2}}{\sigma_{11}^o\varepsilon_{11}^o + \tau_{12}^o\varepsilon_{12}^o} G_C^{XT} \tag{2}$$

where $\delta_{eq}^f$ is the equivalent displacement computed at failure, while the variables $\sigma_{ij}^o$, $\tau_{ij}^o$, *and* $\varepsilon_{ij}^o$ are the effective stress and strain values in the lamina at the onset of damage, used to compute the maximum displacement before failure or cracking. The stress and strain data are generated at the unit volume of the material subject to deformation. The value of energy, $G_C^{XT}$ determining critical deformation at fracture plays an important role in the estimation of the lamina fracture, which is difficult to obtain correctly for fiber direction. The fracture energy value

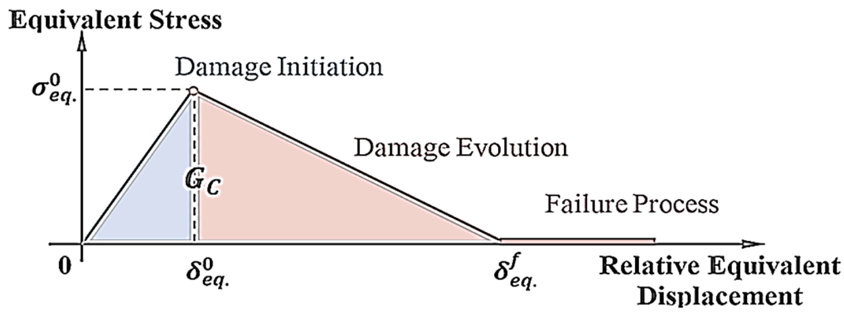


**Fig. 1.** The bilinear elastic-softening constitutive model based on equivalent mixed-mode stress-displacement in UD FRP lamina subject to load in any in-plane directions.

is computed based on the area under stress-equivalent displacement (unit strain) through the elastic to full damage process, equal to the energy required for a material point to undergo cracking phenomena.

An important topic is to define and determine the energy terms in fracture and damage mechanics. In general, cracking and fracture phenomena in material local points are specified as the result of energy exceeding the critical value. Many terms have been used to quantify the cracking process, including strain energy release rate, fracture energy, and fracture toughness [30], etc. The energy that is dissipated per unit cracking surface area through the fracture process is called the strain energy release rate. In energy equilibrium, the energy that is contributed to a crack to further grow is balanced by the amount of dissipated energy caused through the formation of new surfaces. In this respect, the strain energy release rate, $G$ is formulated as:

$$G = -\frac{\partial(U - V)}{\partial A}\left(\mathrm{J}/\mathrm{m}^2 = 0,001\ \mathrm{N}/\mathrm{mm}\right), \tag{3}$$

where $U$ is the potential energy available for crack growth, while $V$ and $A$ are the work related to any external forces acting on the crack regions.

Fracture energy, $G_C$ is defined as the critical value of strain energy release rate, in which, if exceeded, the crack grows ($G \geq G_C$).

Empirically, fracture energy is considered the material property that is independent of the geometry of the structure and the applied loads and boundary conditions. In continuum damage mechanics, the fracture energy parameter is used to trace the softening behavior and predict the mechanism of damage evolution of the material (refer to Fig. 1). Fracture energy of quasi-brittle materials can be obtained by determining the local deformation of materials at fracture, or by a fracture mechanics approach [31]. Therefore, the estimation of the fiber fracture energy, $G_{CF}$ is considered through the calculation of the stress intensity factor.

## 3. The 3-dimensional digital image correlation (DIC) method

In image processing techniques, the DIC method is capable of generating full-field measurements of displacement and strain. Introduced in the 1980s, the DIC method has gained popularity to find application in a broad range of scientific fields, from engineering to medicine and mining [32–34]. The DIC method has also been applied to investigate the failure of composite materials under different loading mechanisms [35–37]. In the following section, the description of a novel 3D DIC setup used in the present work, as well as a brief review of the fundamental theory, is presented.

The principle of the 3D DIC approach is to look for the maximum correlation within a small area (so-called subsets) at the surface of a specimen in the undeformed (or reference surface) and deformed states [64] (Fig. 2a). Subsequently, the algorithm makes a comparison between the deformed and reference states and calculates displacements and strains using an image-matching rule. A straightforward image-matching process as the “cross-correlation” technique, produces the (in-plane) displacement fields u(x,y) and v(x,y) by matching different areas of the two pictures. Fig. 2b shows the test sample with applied speckles for image processing to calculate the cross-correlation coefficient.

A constant displacement rate of 0.5 $mm/min$ was applied to the specimen using a universal Instron machine (Instron MA US) of 100 $kN$ Capacity. During the experiment, two charge-coupled device (CCD) cameras (Basler PiA2400–17gm) were mounted horizontally below the illumination of a high-intensity flashlight and adjusted to monitor a field of interest on the sample’s surface that was painted with standard

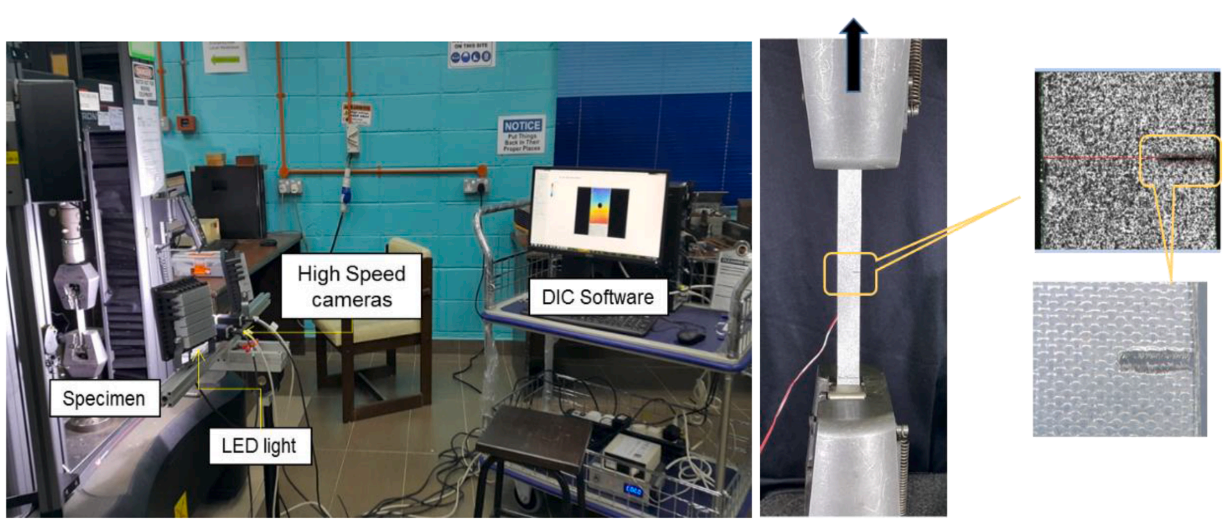


**Fig. 2.** (a) Experimental and DIC system setup, (b) test sample with applied speckles for image processing.

speckle. The two cameras were placed at a 40 cm distance from the test coupon and with a stereo angle of 15° The camera's resolution was 2456 × 2058 Pixels (having 8-bit digitization for grey levels), while a 0.00345 mm/pixel length-pixel ratio was considered for the imaging system. For this test, the CCD cameras were set vertically to the plane (field of interest) of the sample while taking images at a speed of 2 frames/second. The specimen surface was kept in the same plane parallel to the CCD camera during deformation and loading [38]. The system setup was calibrated to transform the image position on the CCDs of two cameras of a specimen surface point to the corresponding coordinates of that point. The calibration procedure aims to set the intrinsic parameters for both cameras of the imaging system, as well as adjust the external position and orientation of the cameras concerning a global coordinate system. In this work, *CorelliSTC software (Holo3, France)* was employed to compute local deformations and strains by using the images collected in the testing program.

## 4. Material and methods

### 4.1. Material and experiment

Five samples with single edge-notch configurations made of UD CFRP composite with $[0]_6$ lay-up are made and used for the experiment. The average sample dimension is listed in Table 1. The samples are fabricated according to ASTM standards [7] with a 5 mm edge-notch length. The test was controlled by a 0.5 mm/Min displacement rate until full failure. The structural response is recorded as a load-displacement curve and used to obtain the properties of the composite. A 3D DIC system is used for full-field measurement of displacement and strain of the CFRP composite surface. The result is used to measure the strain field around the notch tip and estimate the unit deformation of fibers at the final fracture. The fiber fracture energy is then calculated using the deformation at fracture based on the damage mechanics concept.

### 4.2. Finite element modelling

In the computational work, a systematic approach is taken to develop three different finite element (FE) models and to highlight the study's aim in determining the fracture energy and features of the fiber bundle in the form of FRP lamina. In this regard, FE models with three different configurations were systematically generated in the commercial software ABAQUS/Implicit, as shown in Fig. 3a-c. Model-1 was developed as a plain FRP lamina with gripping, in which the dimensions were similar to the experimental sample (refer to Table 1), and the notch was not considered. Model 2 was generated similarly to the experiment. Model-3 was created based on a single edge-notch composite, however, the material part along the notch was removed. The length and thickness of each model were the same as the experimental test according to ASTM standards [5,6]. The deformable 3D shell element (SC8R: 8-node quadrilateral in-plane continuum shell) was used to model the lamina, and a rigid 3D element (R3D8 element) was assigned to the gripping area.

Fig. 4a shows the mesh configuration of the samples, indicating higher mesh density in the sample gripping area (tab region) as well as the notch area, enabling accurate mechanical variables in stress concentration zones. To ensure the accuracy of FE model results, independent of the mesh density with minimized element size error, a mesh convergence study was performed on the model with elastic-damage definition. Two parameters, including measured von Mises stress at the material point, as well as strain energy of the whole structure, are computed in the model with different mesh densities, as shown in Fig. 4b This enables minimizing the element size error at the material level as well as the global structural response. Computed results signify that a mesh density (element number) of 10,000 provides accurate results with minimized error of <0.5 %; however, this study utilized the FE models with mesh density over 22,000, enabling greater resolution for localized phenomena, as recommended elsewhere [29]. To apply the boundary condition, one end side was fixed vertically and two plane rotational degrees of freedom (free to move in the width direction), and the other side was under displacement rate until fully ruptured following the load and boundary condition during the experiment. The applied loading rate was equal to the experiment (0.5 mm/min). To avoid matrix damage and grip indentation in the gripping area, which was observed in experimental tests, a GFRP tab was used in those regions. An orthotropic model was considered to model elastic behavior and for the prediction of failure mode and material degradation. Hashin's continuum damage mechanism was applied to the lamina specimens.

### 4.3. Hybrid experimental-computational approach

The flowchart of the methodology is illustrated in Fig. 4. The research methodology is developed based on a hybrid approach that links the experimental data and computational findings to explore the internal behavior of the composite specimens obtained through 3D FE simulation.

A 3D DIC equipment eliminating the mesoscale roughness of the CFRP composite to measure accurate data of fiber damage evolution in the form of linear-nonlinear strain variation was used along with the mechanical testing to provide insight for mechanical characterization and explain the damage behaviour of 0°-CFRP composite lamina. Three different FE models were developed to predict the internal mechanical behavior of the test sample, as well as to assist in the accurate estimation of the carbon fiber properties in the form of CFRP lamina. The approach is used to validate the model and simulation process and confirm the validity of the elastic and damage properties of the composite obtained in the study. Two verification steps are defined; first, elastic properties are validated through a comparison of experiment and simulation results, and then the damage properties are verified by experimental data, in which significant help from DIC data to ensure the accuracy of the data is highlighted.

## 5. Results and discussion

### 5.1. Mechanical behavior of single edge-notch FRP lamina structure

To understand the mechanisms of deformation and damage process, the results of the experiment in terms of the load-displacement curve are illustrated in Figs. 5 and 6, which indicate three distinct stages with different structural behaviours. Fig. 5 shows a schematic representation of the *load-displacement signature* of the single edge-notch composite sample under tensile loading conditions, while Fig. 6 presents the data obtained during the experiment. Two distinct magnitudes of stiffness are observed, including an elastic stiffness up to 6 % structural deformation, where no matrix crack occurred (Structure stiffness; $k_S$), and the second is when the matrix crack occurs at the notch tip and propagates

**Table 1**
The geometry of the single edge-notch specimens.

| Specimen Dimension, mm | | | U-Notch Dimension, mm | | | Tab, mm | |
|---|---|---|---|---|---|---|---|
| Thickness | Width | Length | Length | Width | Tip Radius | Thickness | Length |
| 0.89 | 15.05 | 235.79 | 5 | 1.11 | 1.05 | 1.03 | 55.32 |

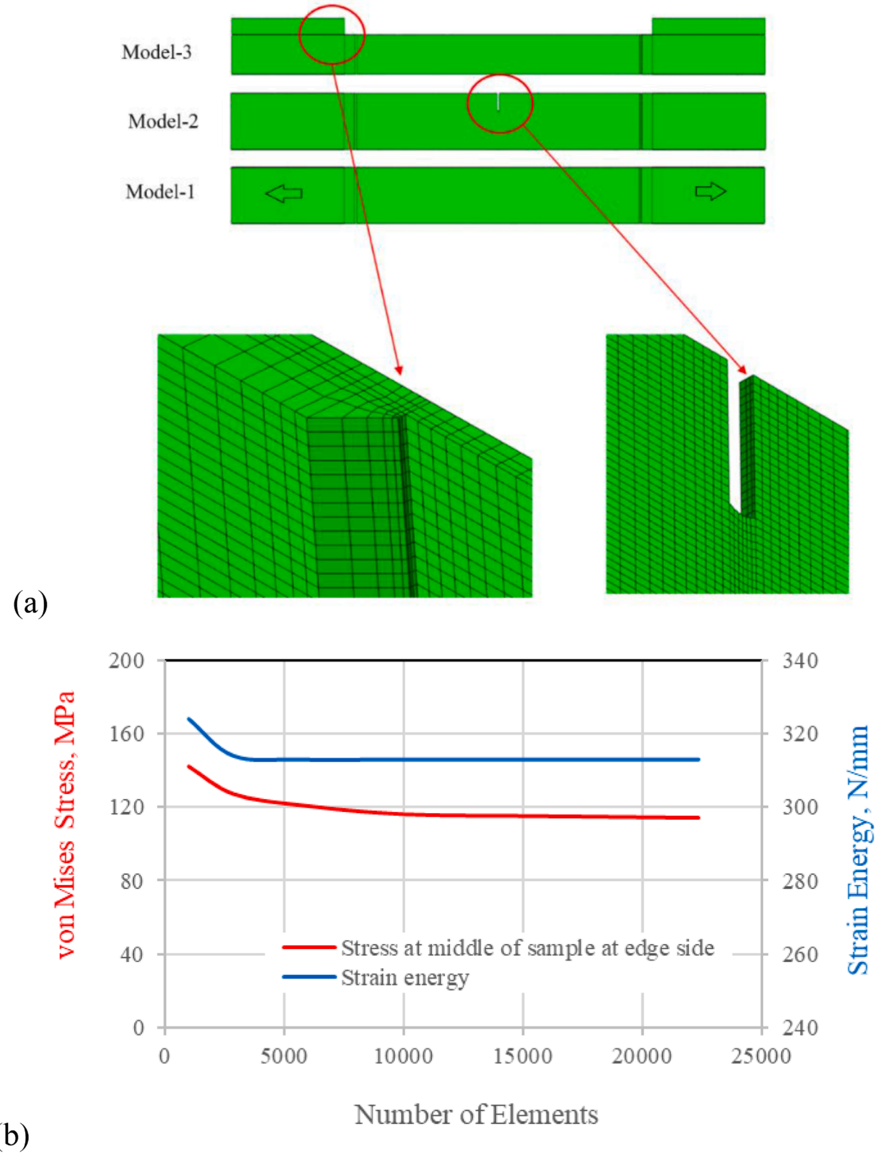


**Fig. 3.** (a) Finite Element models; tensile sample with gripper tap (Model-1), sample with a single edge-notch according to experiment (Model-2), and sample without the notch (Model-3), and (b) mesh convergence study: results of stress value at material point and strain energy of the structure 0.4 mm tensile deformation.

vertically toward the specimen length (Beam stiffness;$k_B$). In the second part, the matrix crack grows, and the single edge-notch specimen is converted to a simple beam under tension loaded up to full failure.

To better understand the overall deformation response of the single-edge notch sample during the tensile test, the experimental results, in terms of the load-displacement curve and the corresponding damage state of the CFRP composite, captured by 3D DIC at various load levels, are shown in Fig. 6 (Top). In this plot, the specimen reaction force data were measured by the testing machine, while the displacement data are directly obtained from the DIC measurement, enabling to definition exact displacement state corresponding to the contour plot of deformation and strain by 3D DIC, as shown in Figs. 6 (Middle, Bottom). It should be noted that the deformation value of the sample measured by the testing machine is an overall displacement of the sigle edge-notch composite structure, which has been presented in Section 5.4 for a comparison to FE results. When the loading started, the structure behaved in an elastic manner up to ≈0.26 mm. An image of the deformation and strain field at the displacement below 0.05 mm (within first stage) was shown in Fig. 6 (Middle, Bottom), indicating a small amount of applied load, caused homogeneous distribution of deformation (concerning notch area) and a constant strain distribution along the structure, however, by increasing the load to the second stage, the contour of deformation and strain at the critical region (0.5 mm displacement) shifted toward the tip of the notch with a crack that propagate vertically along the sample length (deformation distribution follows the crack path). Subsequently, applying a higher load results in the crack propagating further in both up and down directions (3rd image of strain field at 3.8 mm displacement, within stage 3), which upsets the deformation field to vary too. At ≈4 mm displacement, with fully grown cracks along the sample length, the deformation field in the remaining part of the sample is distributed as a normal beam under tensile load. Eventually, the sample failed due to fiber rupture at the average displacement of 4.2 mm (DIC measurement).

It can be concluded that, three main stages/regions with different mechanical behaviours were determined based on the structural deformation states of 0–0.26, 0.26–1.6, and 1.6–4 mm. Within the elastic regime as the first region, the intact specimen carried load with higher structural stiffness (orange dashed line, Fig. 6 Top), which was disrupted due to a vertical crack growth at the notch side. The second region is where stress accumulated in the crack tip and maximum strain was

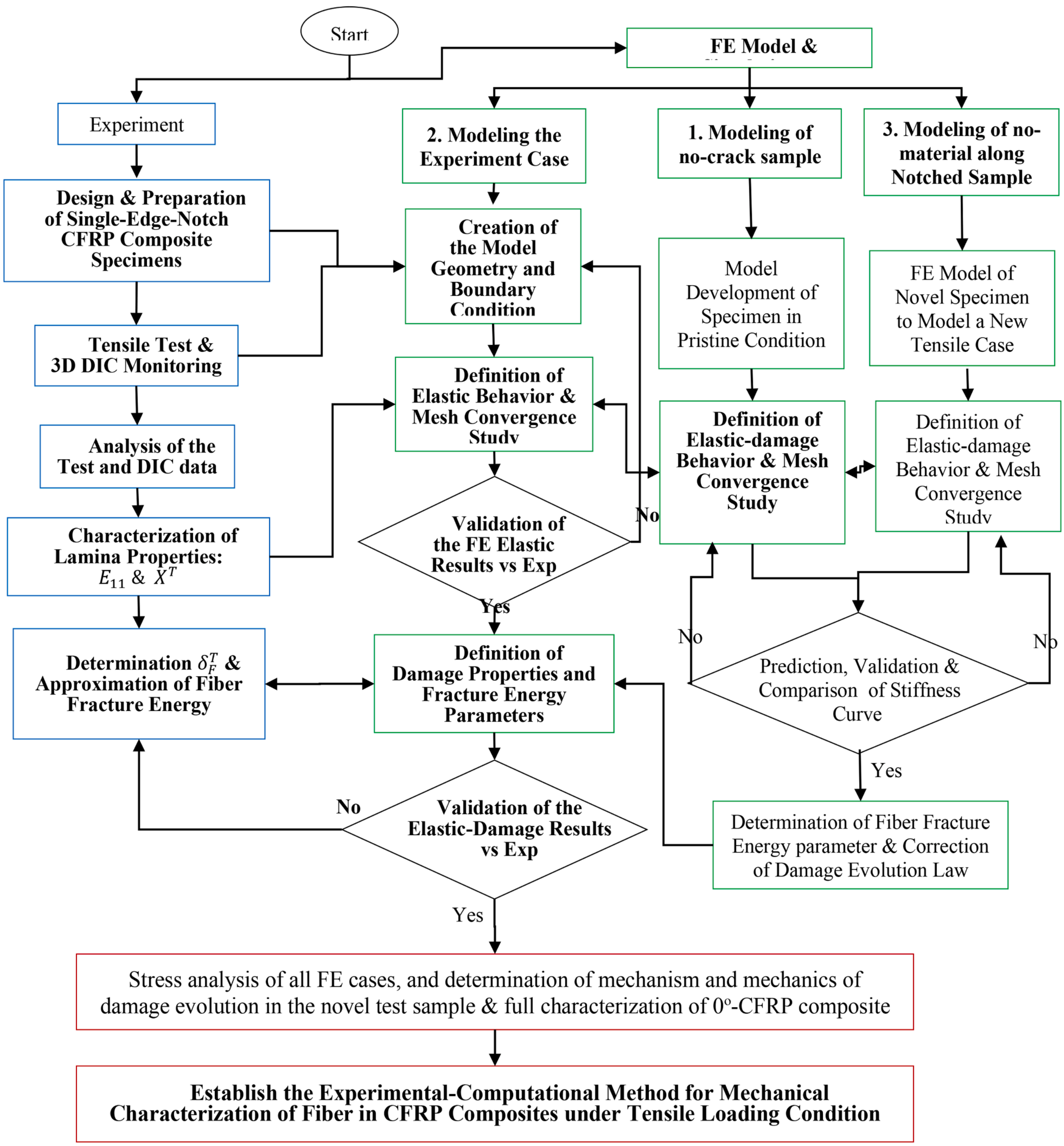


**Fig. 4.** Flowchart of the hybrid experimental-computational approach.

observed with two distinct crack propagations (displacement of 0.26 to 1.6 mm). As the load was applied further, these cracks were gradually and vertically propagated, causing the sample to convert from a notch-to-beam structure, and the accumulation of stress switched to the middle of the beam specimen, with higher shrinkage in cross-sectional area leading to fiber fracture at the middle of the sample. Such mechanical behavior could also be detected by monitoring the deformation field using 3D DIC measurement, as shown in Fig. 6 (Middle). Deformation variation along the y-axis of the sample (along loading direction) highlights the conversion of a single edge-notch sample to a beam with shorter width.

### *5.2. Advantage of the DIC method over the conventional approach*

In order to highlight the advantage of DIC over the conventional method, and also justify the accuracy of the 3D DIC technique, a strain gauge was mounted on the opposite side of the specimen (where was used for DIC measurement was used), and used to measure the strain variation during the tensile test, along with the strain measurement by 3D DIC. Fig. 7 compares the strain vs. time curves of DIC and strain gauge indicating similar trends and values (which serve as evidence for the validity and accuracy of the DIC data), however, the strain gauge data was recorded up to 285 s, where the strain gauge reached its maximum expansion and failed. Detailed information on strain variation was captured by DIC during the elastic regime (up to 60 s) due to the point-to-point focus of DIC, while strain gauge data provides average

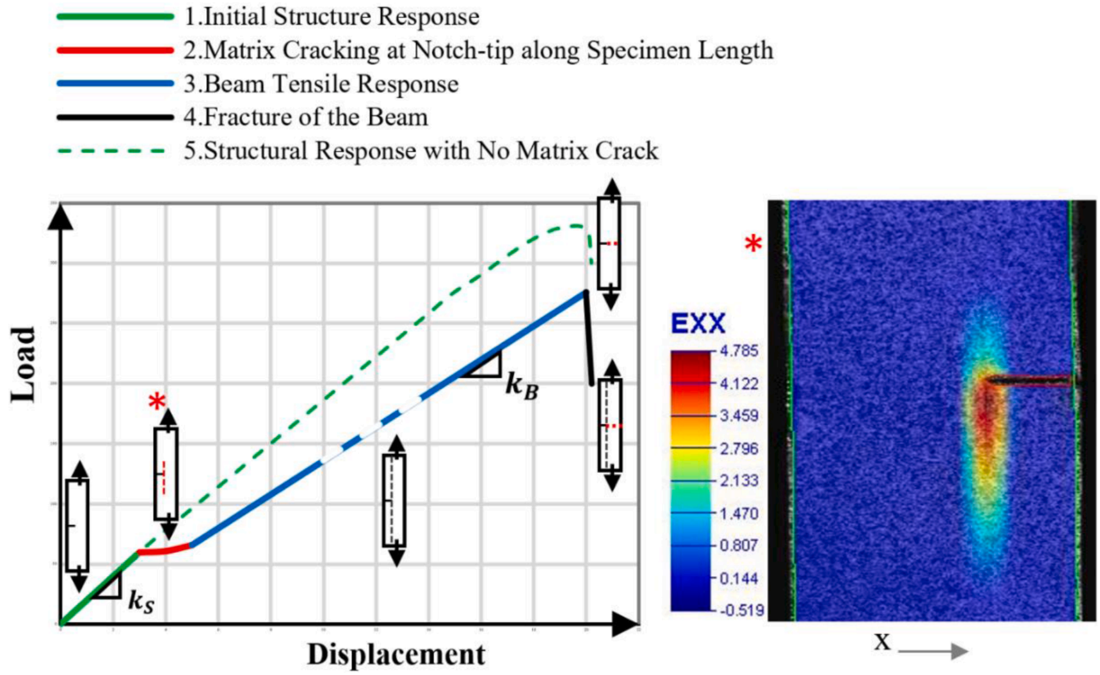


**Fig. 5.** Schematic representation of the load-displacement signature of the single edge-notch UD composite laminate under tensile loading conditions.

data beneath the gauge. The advantage of DIC data is clear due to the provision of long-range data from elastic to damage and full failure that could potentially be used to determine the exact value of stress to determine the stress-strain behaviour.

### 5.3. The use of 3D DIC data to determine material properties

The 3D DIC measurement was used to monitor the deformation variation of the sample at the width (and cross-section) of the sample in the notch site, as shown in Fig. 8 (spackled specimen image on the right side). Two points (red dots) on the right and left of the notch cross-section were selected, and the speckles were traced over time (Fig. 8a). A path between the red dots where also selected to trace the deformation of the sample, as shown in Fig. 8b Fig. 8a shows the displacements of the points as the structure was loaded upward to the full failure stage. The right point has a positive displacement, whereas the left point shows the displacement in a negative sign, indicating further loading of the crack tip side, causes the cross-section to shrink with the appearance of micro necking at the same site. Both points show a similar nonlinear rate of displacement growth, indicating an approximate occurrence of localized damage when a sharp change in displacement growth rate is seen. Fig. 8b shows the reductions of width and cross-section of the specimen at the notch area, which are nonlinearly increased as the structure is loaded further to the failure stage. It is worth mentioning that, the use of 3D DIC measurement in detail/accurate data collection would significantly help in the analysis of the mechanism of deformation in structures with complex geometry.

It can be seen that the rate of reduction in cross-section is higher than the width area. More importantly, the final value of the cross-section was used to determine lamina strength, which was determined to be 2003.5 MPa.

Fig. 9a shows the vertical displacement of the selected points along the specimen length with different original lengths of 2, 10, and 18 mm during the loading. The purpose of this study was to verify the accuracy of the extracted strain from different points through the DIC technique. The figure shows acceptable results obtained from this method, and it could be a good guideline for calculating the strain from this method. Fig. 9b shows the determined modulus of elasticity along the longitudinal direction of the test samples. The average longitudinal Young's modulus of UD CFRP composite with $[0]_6$ lay-up is 78 GPa. Moreover, Fig. 10b shows that the calculated longitudinal Young's modulus with 10 mm and 18 mm returns a more stable value. Based on the Saint-Venant principle, the value of elastic modules should be taken from a point that is far enough (distance) from the critical region. The results of 12 and 18 mm points are converged; therefore, it can be said that after 12 mm from the crack tip, the results are more reliable.

Fig. 10a shows damage factors based on Hashin's damage model in strain-based form. The strain values were measured by the 3D DIC method and used in the calculation of the damage factor. The damage factor of fiber under tensile load, $d_f^t$ can be calculated using a simplified form of Eq. (1), based on strain (by neglecting the effect of shear stress ($\tau_{12} = 0$) as the CFRP specimen prepared having zero degrees, caused minimum shear strain subjected to tensile load) as:

$$d_f^t = \frac{\widehat{\varepsilon_{11}}}{\varepsilon_f^T} \tag{4}$$

where $\widehat{\varepsilon_{11}}$ is the applied strain, and the maximum strain of fiber under tensile, $\varepsilon_f^T$ was obtained 0.015 (see Figs. 7 and 10a), which in theory is the strain at the damage initiation state. Fig. 10b shows the maximum unit deformation for displacement at failure, $\delta_{eq}^f$ (Eq. (2)) using DIC data. Unit deformation indicates deformation at an element with a unit dimension (representing a unit strain value), measured by monitoring displacement at two points (red dot in sample image, *point 1 at top*). By using this value taken from the DIC method, the fracture energy can be calculated using Eqs. (2) and 3. The calculated fracture energy in this study is 31 N/mm. Table 2 lists the average value of mechanical properties obtained from the test using DIC data, indicating <1 % deviation.

### 5.4. Prediction of the mechanical response of 0° single edge notch CFRP composite laminate

Using the proposed hybrid experimental-computational method (see subSection 4.3), the material characterization of the 0°-UD CFRP composite ($[0]_6$ lay-up) was established using a unique single edge- notch sample, mechanical testing assisted with a novel 3D DIC measurement,

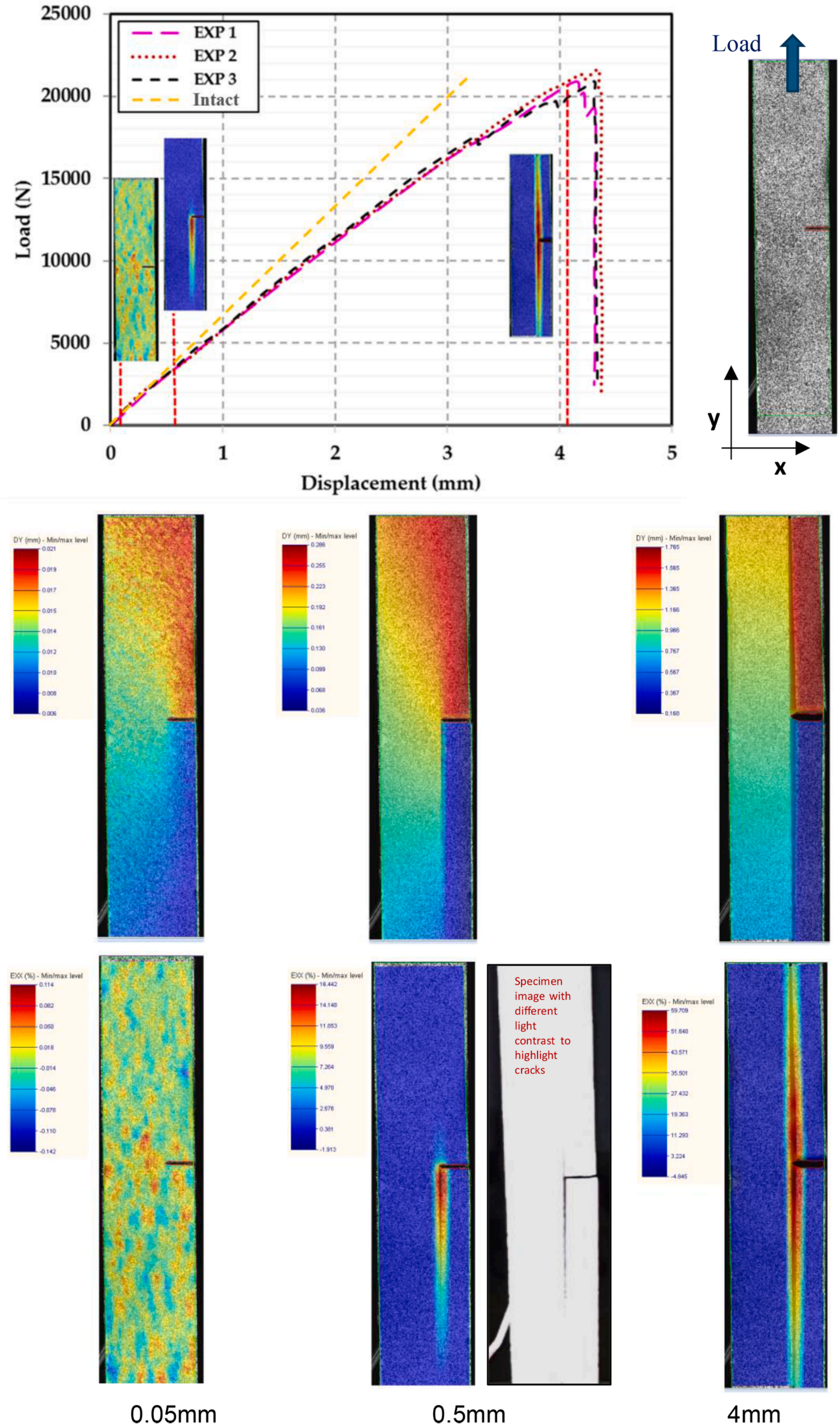


**Fig. 6.** Load-displacement response of a single edge-notch UD 0 CFRP composite under tensile loading (Top), and mapping 3D DIC vertical deformation (Middle) and horizontal strain (Bottom) contours based on different states of displacement of 0.05, 0.5, and 4 mm.

along with a data provided from three FE models covering different case scenarios of the composite sample with various structural feature, to evaluate the tensile behaviour of the composite. Material properties of CFRP lamina were obtained (Table 2) and used in all the simulation processes. Fig. 11 shows the results of three different FE models (refer to Fig. 3, also explained in the flowchart shown in Fig. 4) and compares them with the average result of the experimental. It should be noted that the average experimental data is the actual data obtained by the testing

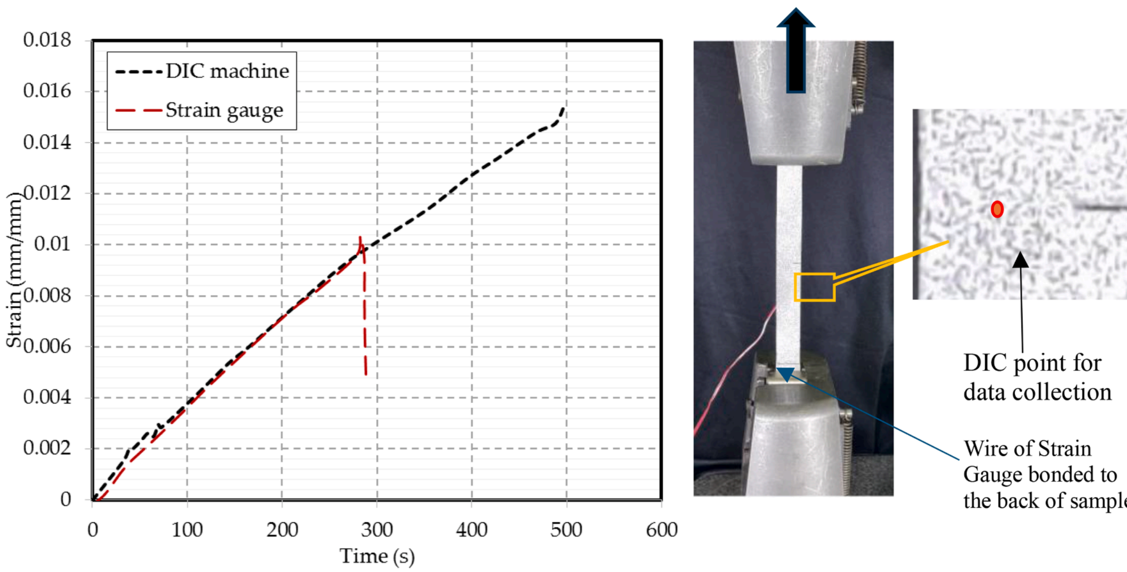


**Fig. 7.** Comparison of the continuous strain variation at the center side of the CFRP composite specimen measured by 3D DIC and strain gauge (left: specimen installation and points for data collection).

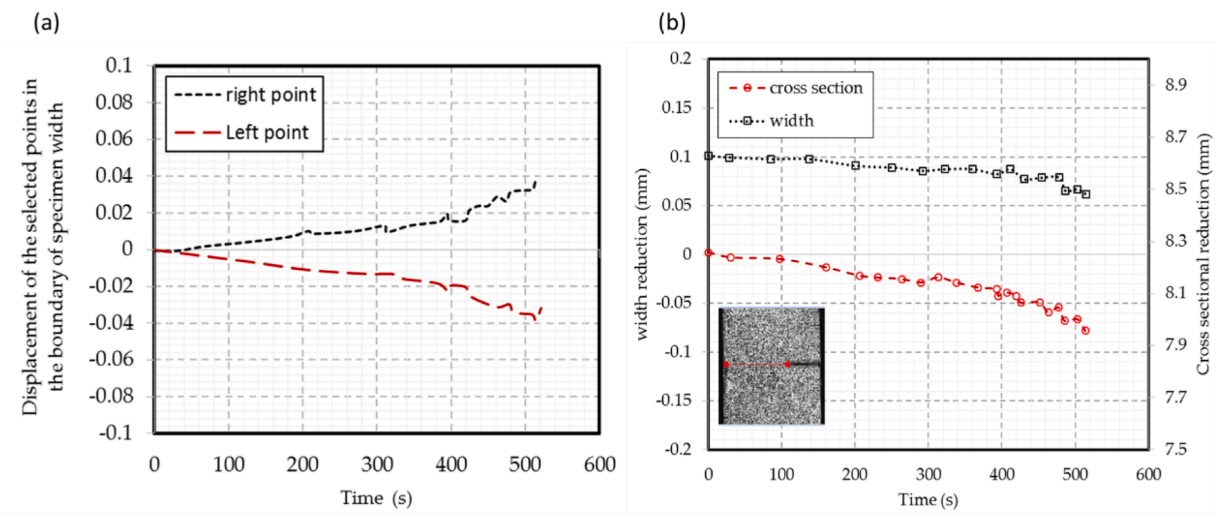


**Fig. 8.** Effect of the width and cross-sectional reduction for the notched specimen over the testing time.

machine, in comparison with the FE models that were built up exactly similar to the load and boundary conditions during the test.

As can be seen in Fig. 11, Model-1 represents the specimen without a notch and shows that the specimen in pristine condition has a large average stiffness of 8 kN/mm. Model-2 was developed to predict linear-to-nonlinear structure behavior in the stage one to stage 2 transition (shown in Fig. 6), where the material behaves within the elastic regime and goes into damage phenomena with two distinct vertical matrix cracks at the notch site. Results of Model-2 in terms of load-displacement response show an accurate prediction of the structure's behavior with <2 % error throughout the test. Mode-3 was used to predict the structural behavior in stage 3 when the structure switched to a beam subjected to a tensile test (refer to Fig. 6) while examining the fracture properties and behavior. In this regard, this model was run for two cases, first with the fracture energy of fiber obtained in this study (31 N/mm, Table 2), and also with the fracture energy parameter reported for the same material in the literature (81.5N/N/mm, [39]). Results in terms of load-displacement curve of the specimen at fracture state are shown in Fig. 11 (right, top), named as "FEM Mode-3E31" and "FEM Mode-3E81.5". The mechanical properties obtained through DIC provided precise predictions of the 0°-CFRP composite failure. It should be noted that this effect may seem small in the prediction of UD lamina, however, the error will get much higher in complex structures with multidirectional orientation and a complex fiber failure at different layers [14].

Another interesting result is to illustrate the variation of the structural stiffness that is affected by different states of internal damage in the structure. Such results are measured experimentally and also by 3D simulation, as depicted in Fig. 12. In this regard, a precise prediction of the test data confirms the validity of the FE model as well as the accuracy of the data obtained through this study. Structural stiffness of the beam structures (Models 1 and 3) shows a linear variation from the beginning to failure states (4 to 7 % changes), for example, from 8.25 to 7.9 kN/mm in Model-1 (5.8 to 5.4 kN/mm in Model-2). This indicates the material linear response affected by the structural deformation. It is worth mentioning that the existence of the notch reduces the structural stiffness up to 30 % (8.1 to 5.7 kN/mm at 2 mm displacement). It is worth mentioning that, prediction of the structural stiffness in certifying the accuracy of the damage model and material properties is often more important compared to the load-displacement curve due to the

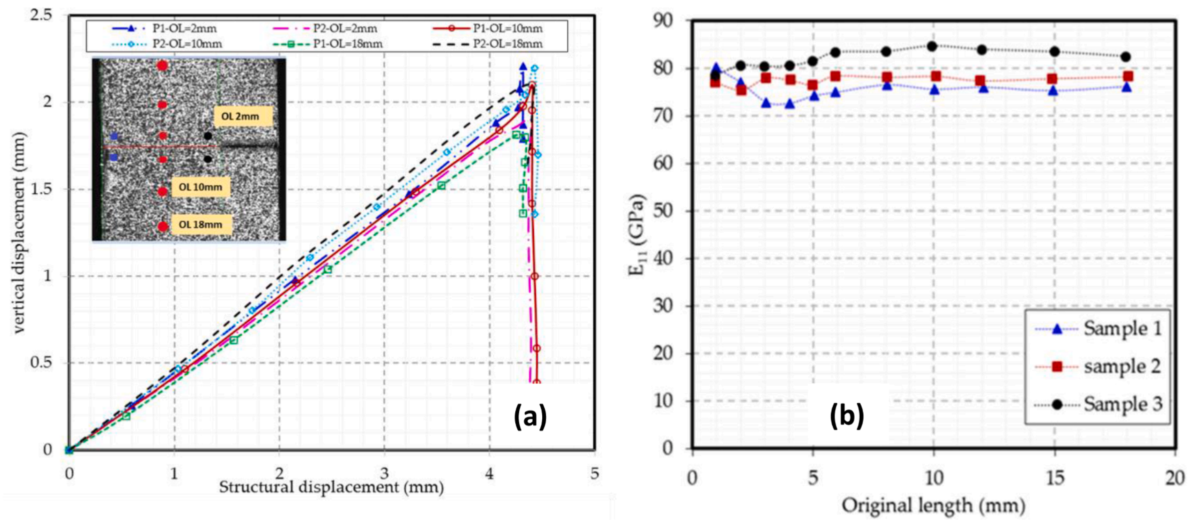


**Fig. 9.** (a) The vertical displacement of the selected points with different original lengths, (b) the longitudinal modulus of elasticity of UD CFRP lamina.

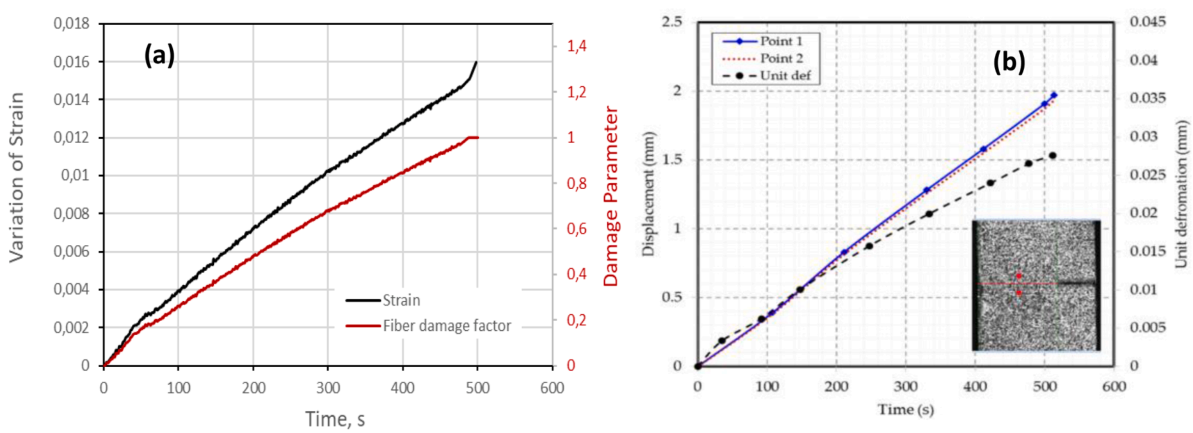


**Fig. 10.** (a) Variation of strain at the center of the specimen and its corresponding damage factor, (b) the unit deformation for displacement at failure.

**Table 2**
Mechanical properties of 0°-CFRP composite lamina obtained through experiment and the use of 3D DIC data.

| Elastic Modulus | Fiber Tensile Strength | Fiber Tensile Fracture Energy | Displacement at Damage Initiation | Displacement at Failure |
|---|---|---|---|---|
| 78.5 GPa | 2003.5 MPa | 31 N/mm | 0.0253 mm | 0.031 mm |

reflection of stiffness response by damage phenomena and formation of complex structural deformation.

It can be inferred that the experiment data and internal FE simulation analysis of the model confirmed three-stage stiffnesses that are changed based on elastic-to-damage behavior of the structure, which could be distinguished by structural deformation ranges of 0–0.26, 0.26–1.6, and 1.6–4 mm (Fig. 12, red vertical dashed line). In the first stage, the single-edge-notch structure behaves elastically, while the second stage is dedicated to notch cracking in terms of vertical matrix failure, which changes the structure from a single-edge-notch to a low beam structure. In stage 3, stiffness changes are followed by Model-2 confirming the structure to behave as a beam element, enabling the data to be used for material characterization. Results of the FE model provided sufficient information through internal analysis and realization of the structure's behavior in the experiment.

## 6. Conclusions

This research contributes to developing a new experimental-computational approach to elaborate on the mechanics of deformation and the mechanism of damage in a specially prepared UD 0°-CFRP laminated composite while characterizing its mechanical properties through elastic-damage behavior. It is shown that, the low intrinsic characteristics of the matrix in CFRP lamina, in comparison to the significantly higher properties of the fibers, resulted in the 0°-lamina properties being predominantly determined by the properties of the fibers. The determination of the elastic characteristics of fibers has been achieved using standardized testing methods. However, numerous challenges have been faced in the characterization of fiber damage and fracture processes. This study involves conducting a tensile experiment on a single edge-notch 0°-CFRP composite lamina. A novel 3D DIC equipment is employed for real-time monitoring of the deformation field at material local points (indicating the fiber behavior), to observe and analyze the strain variation and failure mechanisms during the experiment. A methodology in the form of a hybrid experimental computational approach is proposed that provides insight into the mechanism of deformation and damage of the composite structure. This approach involves the creation of a validated FE model to simulate the test case, as well as additional cases of an innovative FE model, in support of explaining the mechanical behavior of the real composite sample. The results of the model are then utilized to derive and authenticate the

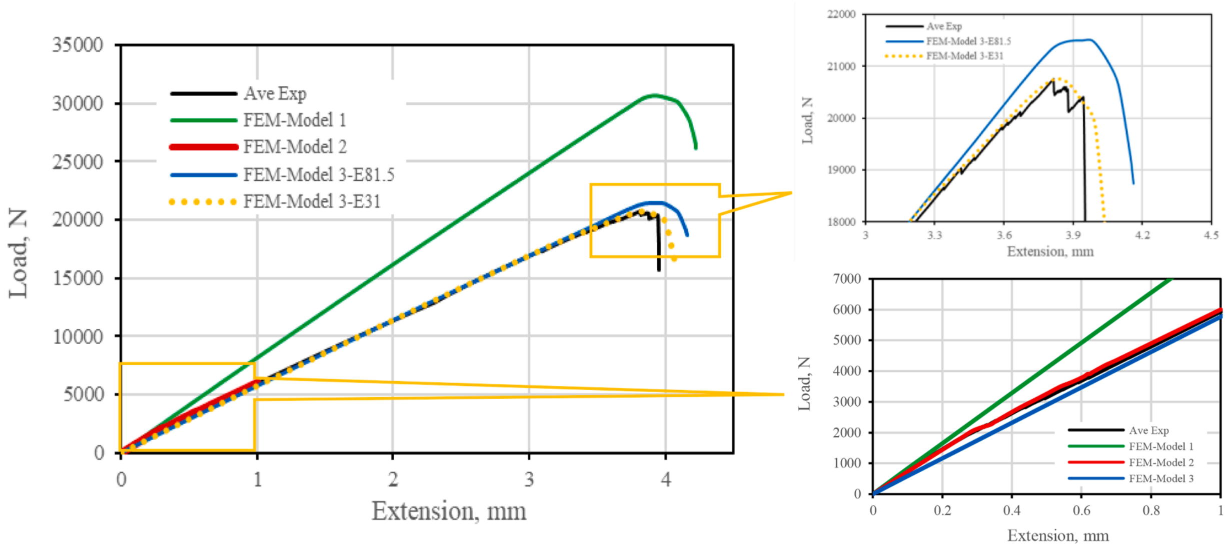


**Fig. 11.** Comparison between experimental data with different FE case scenarios in terms of load-displacement.

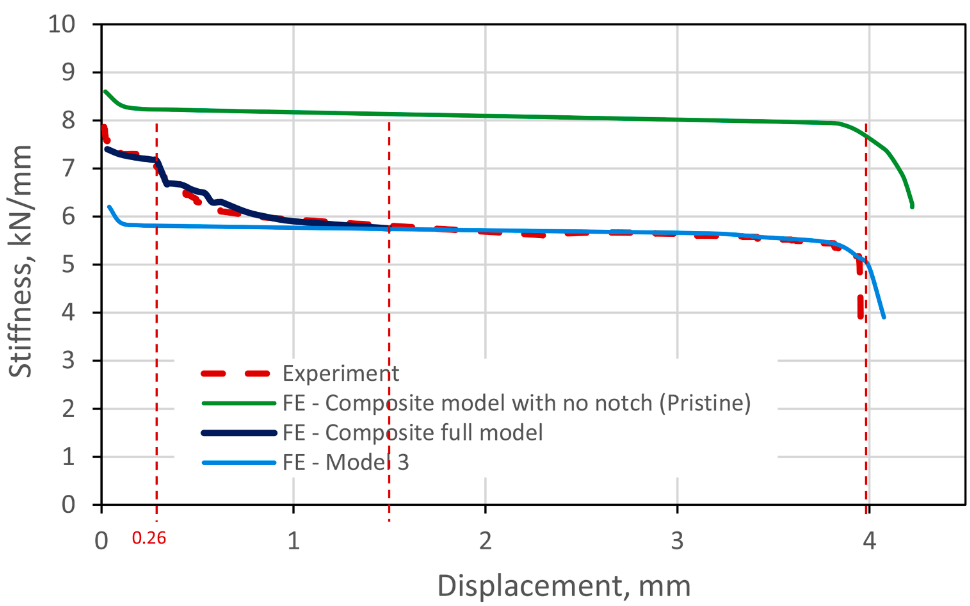


**Fig. 12.** Prediction of structural stiffness determined through the experiment and FE simulation.

damage evolution factors in the fiber bundle in the form of CFRP lamina. The hybrid approach successfully enables obtaining the elastic and damage properties of the lamina in the fiber bundle, recommending a single test combined with the 3D DIC method and FE models in determining the full behavior of 0°-FRP composite lamina. Validated FE data by experiment, distinguished three stages of structural stiffness and behaviors within 0–0.26, 0.26–1.6, and 1.6–4 mm structural deformation, which was used to determine the elastic to damage properties of the CFRP lamina. Emphasis is given to the use of the test, DIC analysis, and FE approach in the characterization of any 0°-FRP composites.

### *6.1. Recommended future study*

A validated mechanical characterization of laminated composites is essential to the design of composite structures for aerospace applications. As future research, a similar approach to what is developed in this research could be effectively utilized in the characterization of FRP composite in different orientations subjected to tensile and compressive loads, as well as shear loads. In addition, the usage of 3D-DIC in capturing the effect of surface meso-scale roughness in deformation and strain variations of composite structure subjected to external loads, especially when the structure is fabricated using different manufacturing methods (e.g., automated fiber placement or resin transfer molding) that cause various degrees of surface roughness, is a very important topic to be investigated. Moreover, the current approach could be utilized in mechanical characterization using residual testing of composites that were exposed to preloads such as fatigue, impact, or even heat and environmental conditions.

## CRediT authorship contribution statement

**S. S. R. Koloor:** Writing – review & editing, Writing – original draft, Visualization, Validation, Supervision, Software, Resources, Project administration, Methodology, Investigation, Funding acquisition, Formal analysis, Data curation, Conceptualization. **A. Farokhi Nejad:** Writing – review & editing, Writing – original draft, Visualization, Validation, Methodology, Formal analysis, Data curation. **N. Yidris:** Writing – review & editing, Visualization, Validation, Supervision, Resources, Project administration, Methodology, Formal analysis, Conceptualization. **S.M. Sapuan:** Writing – review & editing, Visualization, Validation, Supervision, Resources, Project administration, Formal analysis, Conceptualization. **M.R. Abdullah:** Writing – review & editing, Visualization, Validation, Resources, Project administration, Funding acquisition, Formal analysis. **M.N. Tamin:** Writing – review & editing, Visualization, Validation, Supervision, Resources, Project administration, Formal analysis, Conceptualization.

## Declaration of competing interest

The authors declare that they have no known competing financial interests or personal relationships that could have appeared to influence the work reported in this paper.

## Acknowledgements

The authors acknowledge the support by Universiti Putra Malaysia under Putra Grant no GP/2018/9635100. The 5th author would like to acknowledge the support from Universiti Teknologi Malaysia for the funding under UTM R&D (R.J130000.77514J509). Also, the authors would like to acknowledge *AIRBUS*, France, *Aerospace Malaysia Innovation Centre* (AMIC), and *Composites Technology Research Malaysia* (CTRM) for the support in providing the aerospace-grade CFRP composite material and novel 3D DIC equipment in a research collaboration with Universiti Teknologi Malaysia (UTM) (under UTM Grant No 4C089 and 01M01). The financial support by Universität der Bundeswehr München for Open Access publication is acknowledged.

## Data availability

Data will be made available on request.

## References

[1] P.E. Irving, C. Soutis, Polymer Composites in the Aerospace Industry, Woodhead Publishing, 2019.
[2] J. Mlýnek, et al., Fabrication of high-quality polymer composite frame by a new method of fiber winding process, Polymers (Basel) 12 (5) (2020) 1037.
[3] S. Murakami, Continuum Damage mechanics: a Continuum Mechanics Approach to the Analysis of Damage and Fracture, 185, Springer Science & Business Media, 2012.
[4] K.J. Wong, et al., Moisture absorption effects on mode II delamination of carbon/epoxy composites, Polymers (Basel) 12 (9) (2020) 2162.
[5] D. ASTM, Standard Test Method For Tensile Properties of Polymer Matrix Composite Materials, ASTM International, West Conshohocken, PA, 2008.
[6] A. International, Standard Test Method For Compressive Properties of Rigid Plastics, ASTM international, 2010.
[7] I. El-Sagheer, et al., An assessment of ASTM E1922 for measuring the translaminar fracture toughness of laminated polymer matrix composite materials, Polymers (Basel) 13 (18) (2021) 3129.
[8] M. Laffan, et al., Translaminar fracture toughness testing of composites: a review, Polym. Test 31 (3) (2012) 481–489.
[9] J. Parmigiani, T. Kennedy, Failure of notched laminates under out-of-plane bending, in: Sixth Annual Technical Review Meeting, FAA Joint Advanced Materials and Structures (JAMS) Center of Excellence, 2010.
[10] M. Laffan, et al., Measurement of the fracture toughness associated with the longitudinal fibre compressive failure mode of laminated composites, Comp. Part A: Appl. Sci. Manufact. 43 (11) (2012) 1930–1938.
[11] K. Honjo, Fracture toughness of PAN-based carbon fibers estimated from strength–mirror size relation, Carbon N Y 41 (5) (2003) 979–984.
[12] M.S. Khan, et al., Representative cell analysis for damage-based failure model of polymer hexagonal honeycomb structure under the out-of-plane loadings, Polymers (Basel) 13 (1) (2020) 52.
[13] S. Koloor, et al., FE model-based construction and progressive damage processes of FRP composite laminates with different manufacturing processes, Int. J. Mech. Sci. 141 (2018) 223–235.
[14] S. R. Koloor, et al., Linear-nonlinear stiffness responses of carbon fiber-reinforced polymer composite materials and structures: a numerical study, Polymers (Basel) 13 (3) (2021) 344.
[15] Y. Wang, et al., Evolution of fibre deflection leading to kink-band formation in unidirectional glass fibre/epoxy composite under axial compression, Compos. Sci. Technol. 213 (2021) 108929.
[16] A. Farokhi Nejad, et al., Hybrid and synthetic FRP composites under different strain rates: a review, Polymers (Basel) 13 (19) (2021) 3400.
[17] R. Gutkin, et al., Modelling the R-curve effect and its specimen-dependence, Int. J. Solids Struct. 48 (11–12) (2011) 1767–1777.
[18] S. Pinho, P. Robinson, L. Iannucci, Developing a four point bend specimen to measure the mode I intralaminar fracture toughness of unidirectional laminated composites, Compos. Sci. Technol. 69 (7–8) (2009) 1303–1309.
[19] N. Azmi, et al., Compressive failure behaviour of glass epoxy and graphite epoxy composite laminates due to the effects of different cut-out sizes and variations in fibre orientation, Mater. Today: Proceed. 48 (2022) 1936–1940.
[20] Y. Geboes, et al., The translaminar fracture toughness of high-performance polymer fibre composites and their carbon fibre hybrids, Compos. Sci. Technol. 221 (2022) 109307.
[21] X. Xu, A. Paul, M.R. Wisnom, Thickness effect on mode I trans-laminar fracture toughness of quasi-isotropic carbon/epoxy laminates, Compos. Struct. 210 (2019) 145–151.
[22] X. Sun, et al., In situ characterization of trans-laminar fracture toughness using X-ray computed tomography, Compos. Commun. 21 (2020) 100408.
[23] X. Xu, X. Sun, M.R. Wisnom, Initial R-curves for trans-laminar fracture of quasi-isotropic carbon/epoxy laminates from specimens with increasing size, Compos. Sci. Technol. 216 (2021) 109077.
[24] Fatigue, A.I.C.E.o. and F.S.E.o.F. Mechanics, Standard Test Method For Linear-elastic Plane-Strain Fracture Toughness K [Ic] of Metallic Materials, ASTM international, 2013.
[25] F. Bongiorno, C. Militello, B. Zuccarello, Mode I translaminar fracture toughness of high performance laminated biocomposites reinforced by sisal fibers: accurate measurement approach and lay-up effects, Compos. Sci. Technol. 217 (2022) 109089.
[26] Y. Saadati, et al., Study of translaminar fracture toughness of unidirectional flax/epoxy composite, Compos. Part C: Open Access 1 (2020) 100008.
[27] J.H. Underwood, et al., Translaminar Fracture Toughness Test Methods and Results from Interlaboratory Tests of Carbon/Epoxy Laminates, 1256, ASTM special technical publication, 1995, pp. 486–508.
[28] T. Uhl, Damage detection in composite materials using hyperspectral imaging, in: European Workshop on Structural Health Monitoring: EWSHM 2022-Volume 2, Springer Nature, 2022.
[29] S. Koloor, M. Ayatollahi, M. Tamin, Elastic-damage deformation response of fiber-reinforced polymer composite laminates with lamina interfaces, J. Reinforced Plastics Compos. 36 (11) (2017) 832–849.
[30] F. Madureira, L.F. da Silva, V. Tita, Compliance methods for bonded joints: part i-investigation of the standardized methods to obtain the strain energy release rate for mode i, J. Adhes. 99 (11) (2023) 1769–1790.
[31] X. Han, et al., Determining the fracture toughness of quasi-brittle materials with notched four-point bending tests, Eng. Fract. Mech. 284 (2023) 109259.
[32] M. Malesa, K. Malowany, M. Kujawinska, Multi-camera DIC system with spatial data stitching procedure for measurements of engineering objects, Photonics Lett. Pol. 6 (4) (2014) 157–159.
[33] S. Dai, X. Liu, K. Nawnit, Experimental study on the fracture process zone characteristics in concrete utilizing DIC and AE methods, Appl. Sci. 9 (7) (2019) 1346.
[34] M. Pellet, et al., Is digital image correlation able to detect any mechanical effect of cranial osteopathic manipulation?–A preliminary study, Int. J. Osteopathic Med. 29 (2018) 10–14.
[35] M. Babaeeian, M. Mohammadimehr, Investigation of the time elapsed effect on residual stress measurement in a composite plate by DIC method, Opt Lasers Eng 128 (2020) 106002.
[36] D. Rahmatabadi, et al., Characterizing the elastic and plastic properties of the multilayered Al/Brass composite produced by ARB using DIC, Mater. Sci. Eng.: A 753 (2019) 70–78.
[37] M. Zhu, et al., Digital image correlation assisted characterization of mode I fatigue delamination in composites, Compos. Struct. 253 (2020) 112746.
[38] B. Pan, et al., Two-dimensional digital image correlation for in-plane displacement and strain measurement: a review, Measurem. Sci. Technol. 20 (6) (2009) 062001.
[39] P.P. Camanho, et al., Hybrid titanium–CFRP laminates for high-performance bolted joints, Comp. Part A: Appl. Sci. Manufact. 40 (12) (2009) 1826–1837.